CEACAM1 Orchestrates Lipid Raft Dynamics and B-cell Receptor Signaling in Mantle Cell Lymphoma

Vu Ngo

vngo@coh.org

Beckman Research Institute, City of Hope https://orcid.org/0000-0002-9501-6990

Serene Xavier

Beckman Research Institute, City of Hope

Vishal Khairnar

City of Hope https://orcid.org/0000-0002-3584-7530

Vivian Nguyen

Beckman Research Institute, City of Hope

An Phan

Beckman Research Institute, City of Hope

Lu Yang

Beckman Research Institute, City of Hope National Comprehensive Cancer Center
https://orcid.org/0000-0001-7952-0399

Michael Nelson

University of Wisconsin-Madison https://orcid.org/0000-0003-0480-5597

Jinhui Wang

City of Hope

Aimin Li

City of Hope/ Beckman Research Institute

Huimin Geng

University of California, San Francisco

Jaewoong Lee

Beckman Research Institute, City of Hope

Teresa Sadras

Beckman Research Institute, City of Hope

Lan Pham

AbbVie Inc.

Dennis Wiesenberger

Department of Pathology, Microbiology, and Immunology, University of Nebraska Medical Center, Omaha, NE, USA

Wing Chan

Beckman Research Institute https://orcid.org/0000-0002-6243-6008

Karl Lang

University of Duisburg-Essen

Geoffrey Shouse

City of Hope National Medical Center https://orcid.org/0000-0002-7917-5713

Alexey Danilov

City of Hope https://orcid.org/0000-0003-4461-0970

Joo Song

City of Hope Medical Center

Markus Müschen

Yale University https://orcid.org/0000-0002-6064-8613

Article

Keywords:

Posted Date: November 1st, 2024

DOI: https://doi.org/10.21203/rs.3.rs-5321424/v1

Additional Declarations: There is **NO** Competing Interest.

Abstract

B-cell receptor (BCR) signaling plays an important role in the pathogenesis of mantle cell lymphoma (MCL), but the detailed mechanisms are not fully understood. In this study, through a genome-wide loss-of-function screen, we have identified carcinoembryonic antigen-related cell adhesion molecule 1 (CEACAM1) as an essential factor in a subset of MCL tumors. Our BCR signal transduction studies revealed that CEACAM1 plays a critical role in BCR signaling by orchestrating two dynamic processes. First, following BCR engagement, CEACAM1 stabilizes membrane microdomains (lipid rafts) by anchoring to the F-actin cytoskeleton through adaptor protein filamin A. Second, CEACAM1 recruits and increases the abundance of SYK in the BCR complex leading to BCR activation. These activities of CEACAM1 require its cytoplasmic tail and the N-terminal ectodomain. Considering that previous studies have extensively characterized CEACAM1 as an ITIM-bearing inhibitory receptor, our findings regarding its *activating* role are both surprising and context-dependent, which may have implications for BCR-targeting therapies.

Main Text:

INTRODUCTION

Mantle cell lymphoma (MCL) arises primarily from transformed pre-germinal center (GC) or GC-experienced B-cells, the vast majority of which carry the t(11;14)(q13;q32) with oncogenic activation of cyclin D1 (*CCND1*). Pathological B-cell receptor (BCR) signaling represents an important driver of malignant transformation in MCL, which is evident from the stereotyped, biased immunoglobulin heavy chain variable region gene (IGHV) repertoire in most MCL cases [1], increased expression of BCR signaling components [2,3], and strong, albeit short-lived, clinical responses to ibrutinib which targets the BCR-downstream Bruton's tyrosine kinase (BTK) [4,5]. With the introduction of ibrutinib, the overall survival of patients has been extended by 5–8 years [6], but MCL remains an incurable disease. Mechanisms underlying BCR hyperactivity have been established in diffuse large B-cell lymphoma (DLBCL) such as activating mutations in components of the BCR pathway [7–9], and in B-cell chronic lymphocytic leukemia (B-CLL) with self-recognition of the BCR [10]. However, little is known about the mechanisms driving aberrant BCR signaling in MCL.

Carcinoembryonic antigen-related cell adhesion molecule 1 (CEACAM1) is a member of the carcinoembryonic antigen (CEA) family of immunoglobulin-like transmembrane proteins and is expressed on lymphocytes, natural killer (NK) cells, granulocytes, epithelial and certain endothelial cells [11,12]. While the N-terminal domain of CEACAM1 typically mediates trans-homophilic interactions, its cytoplasmic tail carries two immunoreceptor tyrosine-based inhibitory motifs (ITIMs), a unique feature among the CEACAM family. ITIMs are signaling domains that recruit the inhibitory phosphatases, src homology 2 (SH-2) domain-containing protein tyrosine phosphatase 1 (SHP-1) and SH-2 containing inositol 5' polyphosphatase 1 (SHIP1), which dephosphorylate BCR and T-cell receptor (TCR) pathway substrates [13]. Of the 109 ITIM-bearing inhibitory receptors in the human genome, normal B cells express CEACAM1, CD22, CD72, paired immunoglobulin-like type 2 receptor beta (PILRB), and the Fc fragment of IgG receptor IIb (FCGR2B). Mice lacking any of the last four of these receptors develop autoimmune disease and B-lymphoproliferation driven by hyperactive BCR signaling [14–17]. However, despite substantial CEACAM1 expression levels on normal B-cells, *Ceacam1*-deficient mice do not develop autoimmune disease; instead, they have significantly reduced rather than increased numbers of B cells [18,19]. These studies suggest that CEACAM1 is functionally distinct from the other ITIM-containing inhibitory receptors on B-cells.

BCR signaling occurs within lipid rafts, which are submicroscopic plasma membrane domains that are rich in sphingolipids, cholesterol and lipid-anchored proteins, including the SRC family kinases LYN, FYN and BLK [20,21]. Antigen engagement leads to recruitment of the BCR to these membrane microdomains, which then quickly coalesce into larger membrane raft regions [22,23]. Clustering of the receptors within the lipid rafts brings them close to the raft-resident kinases, resulting in phosphorylation of two immunoreceptor tyrosine-based activation motifs (ITAMs) in the CD79A and CD79B signal chains of the BCR complex and initiation of downstream signaling cascades [24]. Coalescence of lipid rafts in response to BCR crosslinking is critical for efficient and sustained signaling. Yet, the way in which lipid rafts are stabilized and contribute to hyperactive BCR signaling in MCL remains unclear.

In this study, we identified CEACAM1 as a key factor that supports BCR signaling in MCL through a comprehensive approach combining genome wide CRISPR screens, gene expression profiling and BCR signal transduction studies. Our data shed light on the positive role of CEACAM1 in facilitating BCR signaling in MCL through bolstering lipid-raft functions and orchestrating the actions of signaling components. These findings also provide new mechanistic insights into the dual role of CEACAM1 in the transmission of both activating and inhibitory signals at the BCR complex, depending on the cellular context and coordinated recruitment of signaling molecules.

RESULTS

CRISPR screen identifies CEACAM1 as an essential regulator in MCL

To identify novel molecular targets important for MCL proliferation and survival, we performed an unbiased genome-wide CRISPR library screen [25]. The MCL cell line JEKO-1 was engineered for doxycycline-inducible expression of Cas9 and transduced with a pooled lentiviral CRISPR library of single-guide (sg) RNAs in two replicates. For sufficient coverage of the complex library, we scaled up the library transduction to approximately 500 cells per sgRNA. After transduction and puromycin selection for stable integrants, Cas9 expression was induced for 14 days. Genomic DNA was harvested on days 0 and 14 and subjected to deep sequencing to determine the relative abundance, i.e. depletion or enrichment, of each sgRNA between the two time points. While there was little difference in the abundance of many non-targeting-control sgRNAs between days 0 and 14, sgRNAs targeting genes known to be essential in MCL such as CCND1 [26] and SOX11 [27,28] were substantially depleted by at least 2-fold on day 14 (Fig. 1a, b). To identify additional candidates for further functional analysis, we developed a four-tier filtering strategy. To focus on genes that are specifically expressed in MCL, we first selected for genes that were substantially upregulated in MCL compared to pre-GC B-cells [29] (Z ratio > 0, P < 0.05). In a second step, we selected all genes that were depleted by at least 2-fold (P < 0.01) over the course of the 14-day interval. To orient our search towards genes that could be potential drug targets, we then removed 94 of the selected 435 genes (**Supplementary Table 1**) because they were identified as essential genes in a broad array of cancer cell lines based on a CRISPR screen using the same library [30]. Analyzing clinical outcome and gene expression data from two studies of patients with MCL [31,32], we identified clinical outcome predictors in a final filtering step. To this end, we segregated the clinical cohorts into two equally strong subgroups based on higher vs lower than median mRNA levels for each of the remaining 341 genes. Twenty-one of these genes had a significant association with shorter overall survival of MCL patients in these studies (Fig. 1a). Among the 21 candidates, CEACAM1 had the highest number of depleted sgRNAs (Fig. 1b; **Supplementary Table 2**) and since its function was previously implicated in BCR signaling [19,33,34], we selected this molecule for further study.

We next conducted validation experiments by introducing two CEACAM1-specific sgRNAs identified from the screen into Cas9-expressing JEKO-1 cells. Our findings confirmed that depletion of CEACAM1 led to a decrease in cell viability (Fig. 1c, d). To ensure that the observed reduction in cell viability was not a result of unintended CRISPR-mediated effects on neighboring genes, such as CD79A located at the 19q13.2 locus near CEACAM1, we compared the expression of CD79A between control and CEACAM1 sgRNA-transduced JEKO-1 cells. Our analysis revealed no significant difference in CD79A expression by both flow cytometry and immunoblotting detection assays (**Extended Data** Fig. 1a,b). These results suggest that the reduced cell viability seen in Fig. 1d was not caused by an accidental loss of CD79A expression due to CRISPR-mediated CEACAM1 depletion. Moreover, we investigated whether the impact of CEACAM1 knockdown on JEKO-1 cell viability was linked to the disruption of b-catenin signaling. Previous studies had shown the importance of WNT-b-catenin signaling in MCL [35–37], and it was known that b-catenin interacts with CEACAM1 [38]. However, our results indicated that both control and CEACAM1-knockout JEKO-1 cells exhibited b-catenin stabilization upon IgM stimulation (**Extended Data** Fig. 1c). This stabilization was consistent with increased phosphorylation at the serine 9 residue on GSK3b, leading to the inactivation of this negative regulator of b-catenin (**Extended Data** Fig. 1c). These findings strongly suggested that b-catenin signaling was independent of CEACAM1 in this context. Altogether, our results indicate that reduced cell viability in CEACAM1-depleted JEKO-1 cells was not due to unintended CRISPR-related loss of CD79A or alterations in b-catenin signaling.

To expand the library screen results, we selected a small-hairpin RNA (shRNA) to knock down CEACAM1 (Fig. 1e) and transduced it into multiple lymphoma cell lines. CEACAM1 depletion led to reduced survival in cells with high CEACAM1 expression (JEKO-1, MINO, MAVER-1, and K1718); however, the effect on cell survival was partial in MAVER-1 cells (Fig. 1f). In contrast, depletion of CEACAM1 had little effect on survival of lymphoma cells (SUDHL-6, OCI-LY10, HBL-1, and SSK41) expressing low or undetectable levels of CEACAM1 (Fig. 2d). We extended these results *in vivo* by employing an established xenograft model of MCL using JEKO-1 [39,40]. Two million control or CEACAM1 shRNA-transduced JEKO-1 cells expressing firefly luciferase were intravenously injected into immunodeficient NOD/SCID/IL2R-Gamma null (NSG) mice and tumor growth was monitored by whole-body bioluminescence imaging. All mice showed bioluminescence signals in the spleen, bone marrow and central nervous system, indicating involvement in these organs (Fig. 1g,h). All mice in the control group showed visible bioluminescence by day 14 after tumor implantation and became ill with marked weight loss and hind-leg paralysis, resulting in a median survival of only 37 days. In contrast, mice that received CEACAM1-depleted tumor cells had delayed bioluminescence signals and a median survival of 60 days (Fig. 1i). Collectively, these data indicate that CEACAM1 plays an essential role in a subset of MCL tumors both *in vitro* and *in vivo*.

Table 1
Summary of CEACAM1 IHC staining of tissue microarrays

Disease	Positive	Weak	Negative	Total positive	% Positive
Mantle cell lymphoma	16	4	3	20	86.96%
DLBCL	10	11	61	21	25.61%
GCB	8	7	35	15	30.00%
ABC	0	2	13	2	13.33%
Indeterminate	2	0	15	2	11.76%
Follicular lymphoma	11	15	57	26	31.33%
grade 1–2	4	7	35	11	23.91%
grade 3A	5	5	11	10	47.62%
grade 3B	1	1	1	2	66.67%
DLBCL + FL	0	2	7	2	22.22%
Indeterminate	1	0	3	1	25.00%
Classical Hodgkin lymphoma	2	1	36	3	7.69%

CEACAM1 expression in MCL

To compare CEACAM1 expression levels in other cell types, we re-analyzed previously published gene expression data [29] and found that CEACAM1 mRNA expression is higher in MCL than in normal B cells (Fig. 2a) or other B-cell malignancies (Fig. 2b,c). At the protein level, immunoblot assays showed CEACAM1 is highly expressed in primary MCL samples, in PDX models and in MCL cell lines as compared to non-MCL cells (Fig. 2d). Flow cytometric analysis also revealed high levels of CEACAM1 surface expression on MCL PDX models (Fig. 2e) and primary MCL samples (**Extended Data** Fig. 2a) compared to other B-cell lymphoma or $CD19^+$ naïve B cells. Consistent with a previous report [19], we observed higher CEACAM1 expression levels in $CD27^+$ memory B cells as compared to naïve B cells from three healthy donors (**Extended Data** Fig. 2b). Furthermore, using immunohistochemistry (IHC), we compared CEACAM1 expression in tissue microarrays of different B-cell malignancies. CEACAM1 was found to intensely stain the surface of the lymphoma cells from a majority of primary MCL biopsies (86.9%), and some cases of DLBCL (25.6%), follicular lymphoma (FL) (31.3%), and classical Hodgkin lymphoma (cHL) (7.7%) (Fig. 2f, Table 1).

Because the CEACAM1 antibodies used in immunoblotting (Santa Cruz Biotechnology, clone E-1) and IHC (Abcam, clone EPR4049) only recognize the long isoforms of CEACAM1 while the CEACAM1 antibody used in flow cytometry (eBioscience, clone CD66a-B1.1) recognizes the ectodomain of CEACAM1, CEACAM3, CEACAM5, and CEACAM6, we further clarified which CEACAM members are expressed. To do this, we performed qPCR assays using Taqman probes specific for five CEACAM1 isoforms (**Extended Data** Fig. 3a) and other CEACAM molecules. The Taqman probes were validated for their specific detection of the corresponding CEACAM molecules in the $CEACAM^+$ A549 cell line, using HEK-293T as a negative control (**Extended Data** Fig. 3b). Our data indicate that MCL mostly expresses CEACAM1 long cytoplasmic-tail (CT) isoforms, with low to undetectable levels of CEACAM1 short CT isoforms and undetectable levels of CEACAM3, CEACAM5 and CEACAM6 (**Extended Data** Fig. 3c,d). We also found that CEACAM1 long isoform was predominantly expressed in the marginal zone lymphoma (MZL) cell line Karpas-1718 (K1718) and modestly expressed in the activated B-cell (ABC) DLBCL cell line HBL1 (**Extended Data** Fig. 3c). Together, these data indicate that CEACAM1 is highly expressed in the majority of MCL tumors compared to other CEACAM molecules.

CEACAM1 is required for BCR signaling in MCL

To determine whether CEACAM1 contributes to BCR signaling in MCL, we compared Ca^{2+} release in response to BCR engagement in CEACAM1-deficient JEKO-1 MCL cells and controls. Knockdown of CEACAM1 resulted in markedly reduced Ca^{2+} signals and decreased phosphorylation of the BCR-proximal kinases LYN and SYK, as well as downstream pathways including ERK, PLCG1, and AKT (Fig. 3a-c). BCR-mediated Ca^{2+} signals were also significantly reduced after CEACAM1 depletion in MAVER-1 cells and in the MZL cell line K1718, both of which express high levels of CEACAM1 (Fig. 3d,e). In addition, compared to mature splenic B cells from wild type mice, *Ceacam1*$^{-/-}$ B cells displayed reduced BCR-mediated Ca^{2+} signals (Fig. 3f). These results suggest that CEACAM1 is required for BCR signaling in MCL and normal B cells. To investigate further, we evaluated the association between CEACAM1 expression and BCR signaling activity in MCL. Previous studies have demonstrated that MCL tumors isolated from the lymph node (LN) microenvironment express genes that are correlated with BCR activation, in contrast to tumor cells from peripheral blood (PB) [41]. These results prompted us to re-examine gene expression data from this study and we found that CEACAM1 expression levels were indeed higher in LN-derived MCL cells than in PB-derived MCL cells (Fig. 3g). We next evaluated the correlation between CEACAM1 expression in lymphoma cells and their response to ibrutinib, which inhibits the BCR pathway kinase BTK. Lymphoma cells with high CEACAM1 expression were found to be more sensitive to ibrutinib than those with low expression levels (Fig. 3h), except for MAVER-1 cells which had high CEACAM1 expression but were resistant to ibrutinib (see Discussion). Together, these results indicate that CEACAM1 expression is highly correlated with BCR signaling activity.

We next determined which structural features of CEACAM1 are involved in BCR signaling by generating mutant CEACAM1 constructs that contained either mutated ITIM tyrosine residues (CEACAM1-4L-Y493F/Y520F) or lacked the cytoplasmic tail (CEACAM1-4S). The expression of these constructs was verified by immunoblots and flow cytometry (**Extended Data** Fig. 4a-c). To evaluate the impact of different CEACAM1 variants on BCR signaling, we introduced full-length CEACAM1-4L, CEACAM1-4L-Y493F/Y520F, or CEACAM1-4S into JEKO-1 cells in which endogenous CEACAM1 had been knocked out (Fig. 3i). Our results showed that only JEKO-1 cells expressing CEACAM1-4L, but not CEACAM1-4L-Y493F/Y520F or CEACAM1-4S, were able to rescue the defective BCR-mediated kinase activities after CEACAM1 knockout (Fig. 3j). Taken together, these results indicate that CEACAM1 plays an active role in BCR signaling in both normal B cells and MCL, and that the ITIM tyrosine residues on the cytoplasmic tail are required for this function.

CEACAM1 stabilizes lipid rafts and promotes F-actin reorganization during BCR activation

Since the cytoplasmic tail is important for CEACAM1 function (Fig. 3j), we hypothesized that molecules that interact with this domain play a key role in the BCR signaling complex. One such candidate is the F-actin binding adaptor filamin A (FLNA) [42], a known CEACAM1-interacting protein [43]. To determine whether FLNA contributes to BCR signaling in MCL, we knocked down FLNA in JEKO-1 cells and performed Ca^{2+} flux assays after BCR stimulation. FLNA depletion significantly reduced both Ca^{2+} signals and cell survival in JEKO-1 cells (**Extended Data** Fig. 5). Expanding on this finding, we examined the lipid-raft signaling microenvironment to determine whether CEACAM1 and FLNA promote BCR signaling through increasing lipid raft function. Control (gNTC) or CEACAM1-knockout (gCC1) JEKO-1 cells were stimulated with anti-IgM antibody, and lipid rafts were isolated by sucrose gradient centrifugation (Fig. 4a). As expected, we detected the two membrane raft markers LYN and flotillin-1 [21] in the raft fraction (fraction I) from all four samples (Fig. 4b). In addition, LYN activation, as detected by the anti-phospho-Y^{416} SRC antibody, was observed in lipid raft fractions from the IgM-stimulated samples in a CEACAM1-dependent manner. CEACAM1 was detected in raft fractions of both unstimulated and IgM-stimulated B cells. Importantly, we found that the levels of FLNA were increased in the lipid rafts of IgM-stimulated cells, but only in the presence of CEACAM1 (0.16 to 0.31) and not in CEACAM1-depleted cells (0.22 to 0.07) (Fig. 4b). As an alternative approach, we used confocal immunofluorescence microscopy to confirm the role of CEACAM1 in FLNA localization and LYN activity in lipid rafts during BCR signaling. In control JEKO-1 cells, FLNA is recruited to the membrane regions that are positive for LYN after BCR crosslinking. In contrast, CEACAM1 depletion significantly reduced FLNA recruitment to LYN-enriched lipid-raft regions (Fig. 4c; **Extended Data** Fig. 6). In addition to impaired FLNA recruitment, CEACAM1 deficiency also had a negative impact on the lipid raft marker GM1 staining and on LYN activation, both of which were restored upon CEACAM1 reintroduction (Fig. 4d).

Because FLNA binds F-actin [42], CEACAM1-dependent recruitment of FLNA to lipid rafts likely involves F-actin reorganization to facilitate lipid raft accumulation. To determine the role of CEACAM1 in F-actin reorganization, we used confocal immunofluorescence to observe the changes in the F-actin network in JEKO-1 cells in which CEACAM1 was deleted. Upon BCR cross-linking, the F-actin cytoskeleton was highly clustered on the cell surface and became detectable by confocal microscopy on control JEKO-1 cells (Fig. 4d). Strikingly, accumulation of the F-actin network after BCR stimulation was markedly impaired in CEACAM1-deficient MCL cells (Fig. 4d). The negative impact of CEACAM1 deficiency on F-actin accumulation after BCR crosslinking was readily rescued when CEACAM1 was reintroduced (Fig. 4d). Taken together, these data indicate that CEACAM1 supports BCR signaling by stabilizing lipid rafts through facilitating the localization and reorganization of structural elements such as FLNA and the underlying F-actin cytoskeletal network, respectively.

CEACAM1 interactions with BCR-proximal signaling components depend on intact tyrosine residues and the ligand-binding N-terminal domain

To further investigate the function of CEACAM1 during BCR activation, we examined the interactions between CEACAM1 and SYK or SHP-1 using two MCL cell lines, JEKO-1 and MINO, both having elevated CEACAM1 expression (Fig. 2d**)**. By employing the proximity ligation assay (PLA), we demonstrated that interactions of CEACAM1 with SYK peaked between 5 and 15 minutes following BCR stimulation and then decreased by 30 minutes both in the JEKO-1 and MINO cell lines. However, increased recruitment of SHP-1 to CEACAM1 was only observed at approximately 30 minutes after BCR crosslinking (Fig. 5a,b). To investigate this further, we used co-immunoprecipitation (co-IP) as an alternative method and found comparable early trafficking kinetics of SYK, while SHP-1 recruitment to CEACAM1 occurred at a later stage following BCR activation in both JEKO-1 and MINO cells. Monitoring SYK activity through its phosphorylation revealed that, in both JEKO-1 and MINO cells, SYK activation peaked at 15 minutes after BCR stimulation and declined by 30 minutes, coinciding with the increased recruitment of SHP-1 to CEACAM1 (Fig. 5c,d).

We next determined which CEACAM1 domains are involved in its interactions with BCR signaling components. To do this, we used CEACAM1-knockout JEKO-1 cells that were reconstituted with either full-length 4L, a mutant Y493F/Y520F, or an N-domain deleted (DN) CEACAM1 construct. We monitored the kinetics of protein-interactions using PLA and co-IP assays after BCR stimulation. As expected, tyrosine phosphorylation on the Y493F/Y520F mutant CEACAM1 was impaired upon BCR crosslinking. In contrast to the 4L CEACAM1, this mutant was also defective in its interactions with FLNA, SYK, and SHP-1 following BCR activation (**Extended Data** Fig. 7). Remarkably, like the Y493F/Y520F mutant, the DN CEACAM1 construct was defective in ITIM phosphorylation after BCR stimulation, despite it having intact tyrosine residues. As a result, DN CEACAM1 failed to interact with FLNA, CD79B, LYN, SYK, or SHP-1 (Fig. 6a). Using the PLA method, we confirmed defective DN CEACAM1 interactions with CD79B, LYN, SYK, and SHP-1 during BCR activation (Fig. 6b,c). The negative impact of the Y493F/Y520F mutant or DN CEACAM1 on interactions with BCR-proximal molecules and BCR signaling was consistently reflected in impaired CD79B association with SYK compared to wildtype 4L CEACAM1, as demonstrated by PLA (**Extended Data** Fig. 8). Therefore, these data indicate that CEACAM1 positively contributes to BCR signaling by initially recruting and activating LYN and SYK at the BCR complex, and subsequently recruiting SHP-1 to dampen the signal. Importantly, these interactions rely on the phosphorylation of tyrosine residues and the presence of the N-domain of CEACAM1.

A dual role of CEACAM1 in BCR signaling

The aforementioned data suggest that CEACAM1 has a positive impact on the early stages of BCR signaling by activating LYN and SYK (Fig. 3b,j; Fig. 5), consistent with a previous report [19]. However, this appears contradictory to other studies proposing that CEACAM1 inhibits antigen receptor signaling in B and T cells by recruiting the negative regulator SHP-1 [34,44–46]. In exploring these conflicting roles of CEACAM1, we noted that the inhibitory functions of CEACAM1 were primarily studied in T cells or B cells lacking CEACAM1 expression, followed by the introduction of CEACAM1. To establish a system comparable with these earlier studies, we selected the MCL cell line Z-138 with low CEACAM1 expression (Fig. 2d, Fig. 3h) and reintroduced CEACAM1 into these cells. Overexpression of CEACAM1 in Z-138 cells did not affect IgM surface expression levels (**Extended Data Fig. 9**). However, CEACAM1-overexpressing Z-138 cells exhibited down-regulated BCR signaling, evidenced by reduced CD79A and SYK phosphorylation after IgM stimulation, compared to the empty vector control (Fig. 7a). Similarly, overexpression of CEACAM1 in the CEACAM1-negative Burkitt lymphoma cell line ST486 did not affect the IgM surface expression (**Extended Data Fig. 9**) but significantly down-regulated SYK activation following BCR stimulation compared to control cells (**Extended Data Fig. 10**). The inhibitory effect of CEACAM1 on BCR signaling was dependent on its cytoplasmic tail, as expression of CEACAM1-4S, which lacks this domain, in Z-138 cells showed no change in SYK and CD79A phosphorylation compared to empty vector control (Fig. 7a).

We then used immunoprecipitation assays to investigate the recruitment of SYK, SHP-1, and SHP-2 by CEACAM1, comparing CEACAM1-overexpressing Z-138 cells with JEKO-1 cells, which were knocked out for CEACAM1 and then re-introduced with the same CEACAM1-4L expression construct. As shown in Fig. 7c, CEACAM1 in Z-138 cells predominantly interacts with SHP-1 and SHP-2, whereas in JEKO-1 cells, it associates more with SYK. This aligns with the observed downregulation of BCR signaling in Z-138 cells, evidenced by reduced SYK phosphorylation upon CEACAM1 overexpression (Fig. 7b**)**. Conversely, re-introducing CEACAM1 into CEACAM1-knocked-out JEKO-1 cells resulted in an increase in SYK phosphorylation compared to controls (Fig. 7b**)**. Furthermore, our complementary PLA approach confirmed significantly more CEACAM1-SHP-1 interactions than CEACAM1-SYK interactions in CEACAM1-overexpressing Z-138 cells (Fig. 7d). Collectively, these findings indicate that CEACAM1 not only plays an activating role but can also act as a negative regulator of BCR signaling in lymphoma cells with low or absent CEACAM1 expression by preferentially binding to SHP-1 instead of SYK.

DISCUSSION

Despite strong evidence supporting chronic activation of the BCR in MCL, the mechanisms driving pathological BCR signaling in MCL are not fully understood. In this study, we have identified the type 1 transmembrane protein CEACAM1 as a crucial component of BCR signaling in MCL and MZL. CEACAM1 facilitates BCR signaling by stabilizing the signaling micro-membrane domains to the F-actin network and by recruiting SYK, leading to an abundance of this critical kinase at the BCR complex. This BCR activating function of CEACAM1 requires the intact N-domain and cytoplasmic tyrosine phosphorylation. We also uncovered two distinct patterns in the recruitment dynamics of CEACAM1 towards BCR-proximal kinases and phosphatases, which correlate with its expression status across different cellular contexts (Fig. 8). This discovery provides compelling evidence to reconcile the previously conflicting roles attributed to CEACAM1.

To dissect the role of CEACAM1 in BCR signaling, we investigated the proteins that interact with CEACAM1. Our initial focus was on FLNA, a structural adaptor protein that interacts with both CEACAM1 and the F-actin cytoskeleton, the latter of which is actively remodeled during BCR activation [47]. Our data indicate that CEACAM1 works with FLNA to properly connect the membrane rafts to the underlying three-dimensional F-actin network, effectively securing the signaling complex for successful BCR activation. This raft-stabilizing model is similar to the “tether and trap” model proposed by Tavano *et al* [48,49]. According to the Tavano model, engagement of the TCR with antigen on antigen-presenting cells leads to FLNA recruitment to the immunological synapse (IS) by binding to the cytoplasmic tail of CD28. This enables actin-based recruitment and trapping of membrane rafts in the IS. Notably, a previous study by Khainar *et al* [50] reported that *Ceacam1*-deficient T cells fail to recruit FLNA to the IS, resulting in reduced proliferation and survival of CD8$^+$ T cells after antigen activation. Thus, the role of CEACAM1 in regulating lipid raft dynamics and facilitating BCR signaling in B cells has implications for TCR signaling in T cells as well.

Our study confirms that CEACAM1 plays an important role in regulating BCR signaling, consistent with previous reports on *Ceacam1*-deficient mice [19,33]. These mice showed a decrease in the number of B cells, especially splenic marginal zone B cells that rely on strong BCR signaling [51], as well as defective SYK kinase activity and insufficient antibody response after antigen stimulation [19]. Our study also revealed a significant reduction in BCR-mediated Ca^{2+} signals in *Ceacam1*-deficient B cells compared to *wildtype* B cells, confirming the critical activating role of CEACAM1 in BCR signaling. The positive role of CEACAM1 is further supported by its dynamic interactions with LYN, SYK, and SHP-1. Specifically, CEACAM1 is found to associate with LYN and SYK in the CD79B vicinity after BCR engagement, thereby heightening the concentrations of these crucial kinases at the BCR complex during peak activation. Subsequently, CEACAM1 increases its interaction with SHP-1, which exerts its regulatory role at the end of BCR activation. Furthermore, our data highlight the requirement of the ligand-binding N-terminal domain of CEACAM1 for phosphorylation of ITIM tyrosine residues, and for CEACAM1 interactions with structural elements and signaling kinases. By using DN CEACAM1 lacking the homophilic interaction, we observed that ITIM tyrosine phosphorylation and CEACAM1 interactions with signaling molecules were impaired during BCR activation. These findings are consistent with the study by Chen *et al* [45] which demonstrated the absence of tyrosine phosphorylation on the cytoplasmic tail of CEACAM1 when mutations (R43G and Q44L) were introduced at the N-terminal domain to abolish homophilic binding.

Despite its demonstrated positive impact on BCR signaling, as shown in our current study and by Khairnar *et al* [19,50], our data also revealed the inhibitory function of CEACAM1 in the lymphoma cell lines with low or no CEACAM1 expression, consistent with previous reports [44–46]. It appears that the molecular basis of this negative role of CEACAM1 hinges on its distinct early interaction with SHP-1, as opposed to SYK, observed in its positive function during the initial stages of BCR activation. The variations in these binding dynamics seem to depend on the specific cellular context dictated by differing CEACAM1 expression status, suggesting the involvement of additional regulatory factors in this process. Identifying these regulators is thus essential for a more comprehensive understanding of CEACAM1's signaling outcomes in various cellular settings. One potential clue from our data is the significant difference in SYK expression levels between JEKO-1 and Z-138 cells. In JEKO-1 cells, high SYK expression may enable SYK to outcompete SHP-1 in binding to CEACAM1, ensuring active BCR signaling. In contrast, in Z-138 cells, SYK is expressed at much lower levels, allowing SHP-2 to outcompete it in binding to CEACAM1 and thereby leading to downregulation of BCR signaling. Further investigations including experimental manipulation of SYK, SHP-1, and SHP-2 levels in their interactions with CEACAM1 should help to clarify how these factors influence BCR signaling.

Nonetheless, the role of CEACAM1 in BCR signaling may have important implications for therapies directed at this pathway. The strong correlation between CEACAM1 expression levels and the BCR signature in MCL tumors (Fig. 3g), and its relationship to ibrutinib responsiveness in MCL and MZL cell lines (Fig. 3h), suggests a potential utility of CEACAM1 as a biomarker of ibrutinib therapy in these lymphomas. However, CEACAM1 expression cannot predict ibrutinib sensitivity in patients with mutations that activate alternative pathways, thus overriding BCR signaling. For instance, the MCL cell line MAVER-1, despite its high CEACAM1 expression, is resistant to ibrutinib (Fig. 3h) due to the presence of TRAF3 deletion [52] and NRAS G12C mutation [53] that activate downstream pathways. Moreover, somatic mutations in BCR pathway components, often found in ABC DLBCL, can affect BCR clustering [7], likely rendering these lymphomas to be less dependent on CEACAM1. Therefore, the combined assessment of CEACAM1 expression levels and mutation analysis may serve as valuable biomarkers for predicting ibrutinib sensitivity in MCL and potentially MZL cases.

MATERIALS AND METHODS

Study design

This study aims to understand the mechanisms of CEACAM1 in supporting BCR signaling in MCL. By identifying CEACAM1 from a CRISPR library screen using JEKO-1 cells and its previously reported role in BCR signaling, we hypothesized that CEACAM1 facilitates BCR activity through interaction with BCR signaling components. The study was designed to confirm the CRISPR screen results and investigate the precise molecular mechanisms of CEACAM1 interactions with BCR-proximal signaling elements. CEACAM1 as a critical gene in MCL was confirmed by gene knockout or knockdown using CRISPR or shRNA *in vitro* and *in vivo*. CEACAM1 mRNA and protein expression were compared in MCL, normal B cells, and other B-cell tumors, using gene expression profiling, immunoblotting, immunohistochemistry, and flow cytometry on primary tumor samples and cell lines. The mechanistic roles of CEACAM1 in promoting BCR signaling was investigated by introducing wildtype or mutant CEACAM1 constructs into JEKO-1 cells from which the endogenous CEACAM1 had been knocked out. In these experiments, the activities of BCR-proximal kinases were examined by immunoblotting, and BCR activation was assessed using Ca^{2+} flux assays. To investigate CEACAM1 interactions with proteins proximal to BCR signaling environment, we used lipid raft fractionation method, confocal immunofluorescence microscopy, immunoprecipitation, and Proximity Ligation Assay on the MCL cell lines JEKO-1 and MINO. All experiments were repeated at least twice.

Cell lines and culture conditions

All cell lines were cultured in RPMI-1640 medium (Life Technologies, Grand Island, NY), supplemented with 10% fetal bovine serum (FBS), 100 IU/mL penicillin and 100 μg/mL streptomycin in a humidified incubator at 37°C with 5% CO_2. Cell lines were commercially authenticated using the Promega GenePrint 10 System.

Primary MCL samples and patient-derived xenografts

Primary cells were obtained from the tumor bank of the Pathology Department of City of Hope as de-identified samples after approval by the Institutional Review Board and prepared as previously described [54]. Cells were cultured in RPMI-1640 medium supplemented with 20% FBS in 37°C CO_2 incubator. MCL patient-derived xenografts (PDX) were obtained from the public repository of xenografts (ProXe.org).

CRISPR library screen

The genome-wide CRISPR library screen was carried out using the Human GeCKO v2 Library, 2-plasmid system (a gift from Feng Zhang; Addgene #1000000049) and following the protocol as described [25]. Quantification of sgRNA depletion or enrichment was performed using the MAGeCK software as described [55]. To validate the screen results, top- and bottom-strand oligos of control (gNTC) or the top 3 CEACAM1 gRNAs were synthesized and cloned into the library backbone plasmid lentiGuide-Puro (Addgene #52963) using a Golden Gate assembly as described [25].

Gene expression profiling

Transcriptome data of selected tissues were downloaded from NCBI GEO (GSE2350 [29], GSE132929 and GSE70910 [41]) and analyzed using R Bioconductor packages for Affymetrix Oligonucleotide Arrays [56]. Raw data (CEL files) were normalized using the Robust Multi-array Average (RMA) method. Z score transformation [57] was used to compare significant changes in gene expression between samples. Data were presented as log2 median-centered intensity or Z ratio.

Cell viability measurement

Cell viability was assessed by flow cytometric analysis for the propidium iodide (PI) negative population. In some experiments, shRNA knockdown vectors co-express eGFP and the fractions of PI-, eGFP + were analyzed by flow cytometry and compared with the early time fractions. A reduction in the GFP + fractions over time indicates reduced cell viability.

Immunoblotting

Cells were lysed in RIPA buffer (1% Triton X-100, 0.1% SDS, 20mM Tris-HCl, 150 mM NaCl, 1 mM EDTA) in the presence of protease inhibitor cocktail (Sigma, St. Louis, MO) and Halt phosphatase inhibitor cocktail (ThermoFisher Scientific) for 30 min. Lysates were cleared by centrifugation and protein concentrations were determined by BCA protein assay (Pierce Biotechnology). Twenty micrograms of lysates per lane were separated by 4–15% SDS-PAGE and immobilized on the nitrocellulose membranes (Thermo Fisher, Waltham, MA) for immunoblotting. Immunoblot signals were developed by a chemiluminescent detection method (ThermoFisher Scientific) and captured by standard autoradiographic films.

Immunohistochemistry

Formalin-fixed paraffin-embedded tissue blocks were sliced into 5 µm thick sections on positively charged glass slides. The slides were loaded on the Ventana IHC automated stainer (Ventana Medical Systems, Roche Diagnostics, Indianapolis, IN) for deparaffinization, rehydration, endogenous peroxidase activity inhibition and antigen retrieval. Anti-CEACAM1 rabbit monoclonal antibody (clone EPR4049, Abcam, Cambridge, MA) was then added to the slides followed by DISCOVERY anti-Rabbit HQ and DISCOVERY anti-HQ HRP detection system (Ventana Medical Systems). The stains were visualized using DISCOVERY ChromoMap DAB Kit and counterstained with hematoxylin (Ventana Medical Systems). CEACAM1 staining was reviewed by two expert hematopathologists (JYS and WCC) and positive staining was determined as > 50% of the tumor cells staining. Regarding the intensity, there were cases that had decreased intensity which were scored as weak.

Xenograft study

Mouse care and experimental procedures were performed in accordance with institutional guidelines and approved protocols from the Institutional Animal Care and Use Committee of the City of Hope. Two days after transduction, two million control or CEACAM1 shRNA-transduced JEKO-1 cells were intravenously injected via tail vein into 6–8-week-old immunodeficient NSG mice (Jackson Laboratories, Bar Harbor, ME). Tumor growth was monitored weekly by whole-body bioluminescence imaging using a Spectral LagoX camera and analyzed with Aura software (Spectral Instruments Imaging, Tucson, AZ).

Intracellular Ca^{2+} measurements

Cells were loaded with 1 µM of Indo-1 (ThermoFisher Scientific) in HBSS medium at 37°C for 30 min then washed once and rested (at 37°C for 15 min) before analysis using a LSRII flow cytometer (Becton Dickinson). In some experiments, cells were also stained with fluorescently conjugated antibodies for surface marker detection at RT for 20 min and equilibrated at 37°C for 15 min before flow cytometric acquisition. Baseline fluorescence was recorded for 1 min followed by addition of anti-IgM antibody and continuous recording for additional 4 to 5 min. Changes in intracellular Ca^{2+} concentration were calculated as ratio of Indo-1 emission wavelengths at 420 nm (bound calcium) and 510 nm (free calcium). Data were plotted against time and arithmetically normalized before display.

Ceacam1 deficient mice

Ceacam1 $^{-/-}$ mice were kindly provided by Nicole Beauchemin (Rosalind and Morris Goodman Cancer Centre, Montreal, QC, Canada) [18]. Mice were maintained on the C57BL/6 background and bred as homozygotes.

Lipid raft isolation

Fifty million cells at 10^6/ml were stimulated with 1 µg/ml anti-IgM $F(ab')_2$ antibody and immediately centrifuged at 900 x g for 4 min. Whole cell lysate (WCL) was then prepared by adding 0.5 ml 1x PBS to the cell pellet and mixing with 0.5 ml lysis buffer (0.5% Triton X-100, 10 mM Tris-HCl, 50 mM NaCl, 10 mM EDTA and protease/phosphatase inhibitors) at 4°C for 10 min followed by brief (10 sec) sonication. For the discontinuous sucrose gradient, 1 ml of WCL was mixed with 1ml of 85% sucrose in the lysis buffer without detergent (TNE) and transferred to the bottom of a 14 x 89 mm centrifuge tube. Diluted WCL was overlaid with 4 ml of 35% sucrose in TNE and followed by 2ml of 5% sucrose in TNE. The samples were centrifuged at 200,000 x g at 4°C for 16 h, after which 1ml fractions were collected from the top of the tube. For immunoblot analysis, 30 µl from each fraction was mixed with 10 µl of 4x SDS sample buffer before denaturing by boiling and separation by SDS-PAGE gel electrophoresis.

Confocal immunofluorescence microscopy and quantitative image analysis

One million cells were grown on 35 mm poly-L-lysine-coated N°1.5 glass bottom dish (MatTek Corp., Ashland, MA) at 37°C in CO_2 incubator for 1 h and stimulated with 2 ug/ml anti-IgM F(ab’)2 antibody (Jackson ImmunoResearch Laboratories Inc., PA, USA) for 4 min followed by fixation in 1.5% paraformaldehyde and permeabilization in 0.1% Triton X-100 for 15 min each at RT. Fixed and permeabilized cells were stained with primary antibodies for 2 h at RT in a humidified chamber. After washing 3x in 1x PBS, cells were stained with fluorescently labeled secondary antibodies for 1 h at RT followed by washing twice in 1x PBS and nuclear staining with 4',6-diamidino-2-phenylindole (DAPI) (ThermoFisher Scientific) for 10 min at RT. Fluorescent images were acquired on an LSM 880 confocal microscope (Leica Microsystems Inc., IL, USA) in Airyscan mode using a 20x 0.8NA objective for 2D collections or a 40x 1.2NA objective for 3D reconstructions. Three-dimensional image reconstructions were visualized using the Imaris 9.5 software (Oxford Instruments, Zurich, Switzerland). Quantitative image analysis of the 20x 2D images was conducted using QuPath V0.2.0m6, an open-source bioimage analysis software [58].

Proximity ligation assay

Proximity ligation assay (PLA) was performed using Duolink® In Situ Detection Reagents Red (Sigma-Aldrich, MO, USA) following manufacturer's instructions. Briefly, one million cells were seeded on 35 mm poly-L-lysine-coated N^{O}1.5 glass bottom dish, stimulated with anti-IgM antibody, fixed, and permeabilized as described above. Cells were then blocked using Duolink® Blocking solution for 1 h at 37°C and incubated overnight in a humidified chamber at 4°C with a combination of two primary antibodies of interest. Cells were then washed twice with 1X Duolink® Wash Buffer A and subject to PLA labeling and amplification procedures according to manufacturer's recommendations. Cell nuclei were stained using DAPI and imaged using LSM 880 with Airyscan FAST confocal microscope (Leica Microsystems Inc., IL, USA). Data were analyzed using QuPath V.0.3.2.

Immunoprecipitation

Cells (3–4 x10^7 per condition) were lysed in 1 ml of IP buffer (50 mM Tris HCl, 150 mM NaCl, 1% Triton X-100, and 2 mM EDTA) supplemented with protease inhibitor cocktail (Sigma-Aldrich, MO, USA) and phosphatase inhibitor (ThermoFisher Scientific, MA, USA) on ice for 30 min. Lysates were cleared by centrifugation at 14,000 xg for 15 min at 4^{O}C. One percent of the lysate (~ 10 µl) was saved as input and the rest was incubated with 1 µg of anti-CEACAM1 antibody (Santa Cruz Biotechnology, TX, USA) or isotype control antibody (SouthernBiotech, AL, USA) together with 30 µl of protein G Sepharose beads (Pierce Biotechnology, MA, USA) by rotation at 4^{O}C for 8 h. Antibody-bound beads were washed 6 times in 1 ml of IP buffer by centrifugation at 8,000 xg for 1 min at 4^{O}C. Washed Sepharose beads were resuspended in 1x sample buffer containing 5% beta-mercaptoethanol, heat-denatured for 5 min at 95^{O}C, and analyzed by immunoblotting.

Statistical analysis

Data are shown as mean ± s.d. unless otherwise stated. Statistical analyses were performed using GraphPad Prism 8 (GraphPad Software Inc., La Jolla, CA). An unpaired, two-sided (unless otherwise stated) T test or Mann-Whitney U test was used to analyze statistical significance between two groups. Significance was considered at $P < 0.05$. Kaplan-Meier survival analysis was used to estimate overall survival of mice and a log-rank test was used to compare the difference between two groups. No animals were excluded.

Additional detailed method descriptions are available in Supplementary Materials S1.

Declarations

List of Supplementary Materials

Supplementary Materials S1

Materials and Methods

Extended Data Fig. 1 to 10

Supplementary Table 1 to 8

Supplementary Materials S2: Quantitative image analysis scripts

Competing interests:

Authors declare that they have no competing interests.

Data and materials availability

All data are available in the main text or the supplementary materials. All research materials generated from this study are available by contacting the corresponding author and completing material transfer agreements.

Funding:

National Institute of Health grant P30CA033572 (Cancer Center Support Grant to City of Hope). National Institute of Health grant P50CA107399 (Lymphoma SPORE Developmental Research Program, VNN). National Institute of Health grant R03CA245996, R01CA262754 (VNN). Concern Foundation grant (VNN). The Leukemia Lymphoma Society Career Development grant (VK). The Alex’s Lemonade Stand Foundation grant (VK). The Lymphoma Research Foundation grant (TS). Howard Hughes Medical Institute grant (MM).

Author Contributions

Conceptualization: VNN, MM. Methodology: SX, VK, VN, AP, LY, JW, MSN, AL. Investigation: SX, VK, VN, AP, LY, MSN, AL, JYS, VNN. Visualization: SX, VK, VN, AP, VNN. Data Curation: LY. Resources: JL, LVP, DDW, WCC, KSL, GPS, AVD, JYS, BBS. Formal analysis: LY, HG. Software: MSN. Supervision: VNN, MM. Writing – original draft: VNN, MM. Writing – review & editing: SX, VK, MSN, JL, TS, DDW, WCC, MM, VNN

Acknowledgements

We would like to thank Nicole Beauchemin for sharing *Ceacam1*$^{-/-}$ mice and John E. Shively for critical reading of the manuscript. This article is dedicated to the memory of Dr. Bernhard B. Singer, whose inspiration and unwavering support sustained the study.

References and Notes

1. Hadzidimitriou A, Agathangelidis A, Darzentas N, et al. Is there a role for antigen selection in mantle cell lymphoma? Immunogenetic support from a series of 807 cases. *Blood*. 2011;118(11):3088-3095.
2. Pighi C, Gu TL, Dalai I, et al. Phospho-proteomic analysis of mantle cell lymphoma cells suggests a pro-survival role of B-cell receptor signaling. *Cell Oncol (Dordr)*. 2011;34(2):141-153.
3. Rinaldi A, Kwee I, Taborelli M, et al. Genomic and expression profiling identifies the B-cell associated tyrosine kinase Syk as a possible therapeutic target in mantle cell lymphoma. *Br J Haematol*. 2006;132(3):303-316.
4. Wang ML, Rule S, Martin P, et al. Targeting BTK with ibrutinib in relapsed or refractory mantle-cell lymphoma. *N Engl J Med*. 2013;369(6):507-516.
5. Advani RH, Buggy JJ, Sharman JP, et al. Bruton tyrosine kinase inhibitor ibrutinib (PCI-32765) has significant activity in patients with relapsed/refractory B-cell malignancies. *J Clin Oncol*. 2013;31(1):88-94.
6. Eskelund CW, Kolstad A, Jerkeman M, et al. 15-year follow-up of the Second Nordic Mantle Cell Lymphoma trial (MCL2): prolonged remissions without survival plateau. *Br J Haematol*. 2016;175(3):410-418.
7. Davis RE, Ngo VN, Lenz G, et al. Chronic active B-cell-receptor signalling in diffuse large B-cell lymphoma. *Nature*. 2010;463(7277):88-92.
8. Lenz G, Davis RE, Ngo VN, et al. Oncogenic CARD11 mutations in human diffuse large B cell lymphoma. *Science*. 2008;319(5870):1676-1679.
9. Ngo VN, Young RM, Schmitz R, et al. Oncogenically active MYD88 mutations in human lymphoma. *Nature*. 2011;470(7332):115-119.
10. Duhren-von Minden M, Ubelhart R, Schneider D, et al. Chronic lymphocytic leukaemia is driven by antigen-independent cell-autonomous signalling. *Nature*. 2012;489(7415):309-312.
11. Hammarstrom S. The carcinoembryonic antigen (CEA) family: structures, suggested functions and expression in normal and malignant tissues. *Semin Cancer Biol*. 1999;9(2):67-81.
12. Prall F, Nollau P, Neumaier M, et al. CD66a (BGP), an adhesion molecule of the carcinoembryonic antigen family, is expressed in epithelium, endothelium, and myeloid cells in a wide range of normal human tissues. *J Histochem Cytochem*. 1996;44(1):35-41.
13. Tsubata T. Role of inhibitory BCR co-receptors in immunity. *Infect Disord Drug Targets*. 2012;12(3):181-190.

14. Muller J, Nitschke L. The role of CD22 and Siglec-G in B-cell tolerance and autoimmune disease. *Nat Rev Rheumatol*. 2014;10(7):422-428.
15. Li DH, Winslow MM, Cao TM, et al. Modulation of peripheral B cell tolerance by CD72 in a murine model. *Arthritis Rheum*. 2008;58(10):3192-3204.
16. Kubo T, Uchida Y, Watanabe Y, et al. Augmented TLR9-induced Btk activation in PIR-B-deficient B-1 cells provokes excessive autoantibody production and autoimmunity. *J Exp Med*. 2009;206(9):1971-1982.
17. Bolland S, Ravetch JV. Spontaneous autoimmune disease in Fc(gamma)RIIB-deficient mice results from strain-specific epistasis. *Immunity*. 2000;13(2):277-285.
18. Hemmila E, Turbide C, Olson M, Jothy S, Holmes KV, Beauchemin N. Ceacam1a-/- mice are completely resistant to infection by murine coronavirus mouse hepatitis virus A59. *J Virol*. 2004;78(18):10156-10165.
19. Khairnar V, Duhan V, Maney SK, et al. CEACAM1 induces B-cell survival and is essential for protective antiviral antibody production. *Nat Commun*. 2015;6:6217.
20. Gupta N, DeFranco AL. Lipid rafts and B cell signaling. *Semin Cell Dev Biol*. 2007;18(5):616-626.
21. Dykstra M, Cherukuri A, Sohn HW, Tzeng SJ, Pierce SK. Location is everything: lipid rafts and immune cell signaling. *Annu Rev Immunol*. 2003;21:457-481.
22. Cheng PC, Dykstra ML, Mitchell RN, Pierce SK. A role for lipid rafts in B cell antigen receptor signaling and antigen targeting. *J Exp Med*. 1999;190(11):1549-1560.
23. Gupta N, DeFranco AL. Visualizing lipid raft dynamics and early signaling events during antigen receptor-mediated B-lymphocyte activation. *Mol Biol Cell*. 2003;14(2):432-444.
24. DeFranco AL. The complexity of signaling pathways activated by the BCR. *Curr Opin Immunol*. 1997;9(3):296-308.
25. Joung J, Konermann S, Gootenberg JS, et al. Genome-scale CRISPR-Cas9 knockout and transcriptional activation screening. *Nat Protoc*. 2017;12(4):828-863.
26. Mohanty S, Mohanty A, Sandoval N, et al. Cyclin D1 depletion induces DNA damage in mantle cell lymphoma lines. *Leuk Lymphoma*. 2017;58(3):676-688.
27. Vegliante MC, Palomero J, Perez-Galan P, et al. SOX11 regulates PAX5 expression and blocks terminal B-cell differentiation in aggressive mantle cell lymphoma. *Blood*. 2013;121(12):2175-2185.
28. Mohanty A, Sandoval N, Phan A, et al. Regulation of SOX11 expression through CCND1 and STAT3 in mantle cell lymphoma. *Blood*. 2018.
29. Basso K, Margolin AA, Stolovitzky G, Klein U, Dalla-Favera R, Califano A. Reverse engineering of regulatory networks in human B cells. *Nat Genet*. 2005;37(4):382-390.
30. Meyers RM, Bryan JG, McFarland JM, et al. Computational correction of copy number effect improves specificity of CRISPR-Cas9 essentiality screens in cancer cells. *Nat Genet*. 2017;49(12):1779-1784.

31. Rosenwald A, Wright G, Wiestner A, et al. The proliferation gene expression signature is a quantitative integrator of oncogenic events that predicts survival in mantle cell lymphoma. *Cancer Cell*. 2003;3(2):185-197.
32. Blenk S, Engelmann JC, Pinkert S, et al. Explorative data analysis of MCL reveals gene expression networks implicated in survival and prognosis supported by explorative CGH analysis. *BMC Cancer*. 2008;8:106.
33. Greicius G, Severinson E, Beauchemin N, Obrink B, Singer BB. CEACAM1 is a potent regulator of B cell receptor complex-induced activation. *J Leukoc Biol*. 2003;74(1):126-134.
34. Lobo EO, Zhang Z, Shively JE. Pivotal advance: CEACAM1 is a negative coreceptor for the B cell receptor and promotes CD19-mediated adhesion of B cells in a PI3K-dependent manner. *J Leukoc Biol*. 2009;86(2):205-218.
35. Rizzatti EG, Falcao RP, Panepucci RA, et al. Gene expression profiling of mantle cell lymphoma cells reveals aberrant expression of genes from the PI3K-AKT, WNT and TGFbeta signalling pathways. *Br J Haematol*. 2005;130(4):516-526.
36. Kimura Y, Arakawa F, Kiyasu J, et al. The Wnt signaling pathway and mitotic regulators in the initiation and evolution of mantle cell lymphoma: Gene expression analysis. *Int J Oncol*. 2013;43(2):457-468.
37. Gelebart P, Anand M, Armanious H, et al. Constitutive activation of the Wnt canonical pathway in mantle cell lymphoma. *Blood*. 2008;112(13):5171-5179.
38. Hu W, Bagramyan K, Bhatticharya S, et al. Phosphorylation of human CEACAM1-LF by PKA and GSK3beta promotes its interaction with beta-catenin. *J Biol Chem*. 2021;297(5):101305.
39. Iyengar S, Ariza-McNaughton L, Clear A, et al. Characteristics of human primary mantle cell lymphoma engraftment in NSG mice. *Br J Haematol*. 2016;173(1):165-169.
40. Klanova M, Soukup T, Jaksa R, et al. Mouse models of mantle cell lymphoma, complex changes in gene expression and phenotype of engrafted MCL cells: implications for preclinical research. *Lab Invest*. 2014;94(7):806-817.
41. Saba NS, Liu D, Herman SE, et al. Pathogenic role of B-cell receptor signaling and canonical NF-kappaB activation in mantle cell lymphoma. *Blood*. 2016;128(1):82-92.
42. Wang K, Singer SJ. Interaction of filamin with f-actin in solution. *Proc Natl Acad Sci U S A*. 1977;74(5):2021-2025.
43. Klaile E, Muller MM, Kannicht C, Singer BB, Lucka L. CEACAM1 functionally interacts with filamin A and exerts a dual role in the regulation of cell migration. *J Cell Sci*. 2005;118(Pt 23):5513-5524.
44. Nagaishi T, Pao L, Lin SH, et al. SHP1 phosphatase-dependent T cell inhibition by CEACAM1 adhesion molecule isoforms. *Immunity*. 2006;25(5):769-781.
45. Chen Z, Chen L, Qiao SW, Nagaishi T, Blumberg RS. Carcinoembryonic antigen-related cell adhesion molecule 1 inhibits proximal TCR signaling by targeting ZAP-70. *J Immunol*. 2008;180(9):6085-6093.

46. Tsugawa N, Yamada D, Watabe T, et al. CEACAM1 specifically suppresses B cell receptor signaling-mediated activation. *Biochem Biophys Res Commun*. 2021;535:99-105.
47. Song W, Liu C, Seeley-Fallen MK, Miller H, Ketchum C, Upadhyaya A. Actin-mediated feedback loops in B-cell receptor signaling. *Immunol Rev*. 2013;256(1):177-189.
48. Tavano R, Contento RL, Baranda SJ, et al. CD28 interaction with filamin-A controls lipid raft accumulation at the T-cell immunological synapse. *Nat Cell Biol*. 2006;8(11):1270-1276.
49. Viola A, Gupta N. Tether and trap: regulation of membrane-raft dynamics by actin-binding proteins. *Nat Rev Immunol*. 2007;7(11):889-896.
50. Khairnar V, Duhan V, Patil AM, et al. CEACAM1 promotes CD8(+) T cell responses and improves control of a chronic viral infection. *Nat Commun*. 2018;9(1):2561.
51. Niiro H, Clark EA. Regulation of B-cell fate by antigen-receptor signals. *Nat Rev Immunol*. 2002;2(12):945-956.
52. Rahal R, Frick M, Romero R, et al. Pharmacological and genomic profiling identifies NF-kappaB-targeted treatment strategies for mantle cell lymphoma. *Nat Med*. 2014;20(1):87-92.
53. Bea S, Valdes-Mas R, Navarro A, et al. Landscape of somatic mutations and clonal evolution in mantle cell lymphoma. *Proc Natl Acad Sci U S A*. 2013;110(45):18250-18255.
54. Mohanty A, Sandoval N, Das M, et al. CCND1 mutations increase protein stability and promote ibrutinib resistance in mantle cell lymphoma. *Oncotarget*. 2016;7(45):73558-73572.
55. Li W, Xu H, Xiao T, et al. MAGeCK enables robust identification of essential genes from genome-scale CRISPR/Cas9 knockout screens. *Genome Biol*. 2014;15(12):554.
56. Gautier L, Cope L, Bolstad BM, Irizarry RA. affy--analysis of Affymetrix GeneChip data at the probe level. *Bioinformatics*. 2004;20(3):307-315.
57. Cheadle C, Vawter MP, Freed WJ, Becker KG. Analysis of microarray data using Z score transformation. *J Mol Diagn*. 2003;5(2):73-81.
58. Bankhead P, Loughrey MB, Fernandez JA, et al. QuPath: Open source software for digital pathology image analysis. *Sci Rep*. 2017;7(1):16878.

Extended Data

Extended data figure 9 not available with this version

Figures

Figure 1

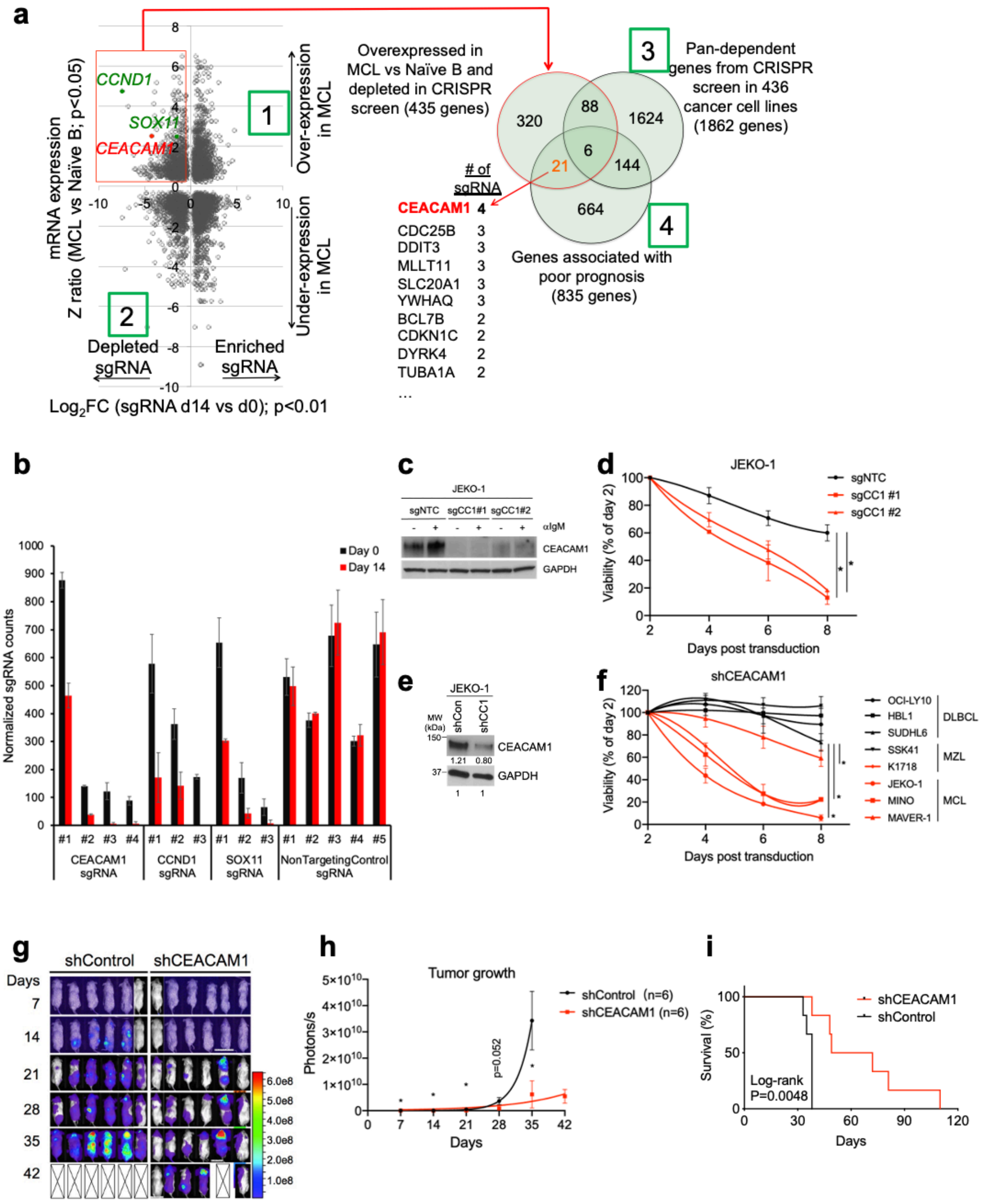

Figure 1

CRISPR library screen identifies CEACAM1 as essential in MCL. a, Analysis of CRISPR library screen results. *Left panel.* Log_2 fold-change of sgRNA counts between day 14 and day 0 (P<0.01; Permutation test) from the CRISPR library screen in JEKO-1 cells are plotted against the Z ratio of mRNA expression between MCL and naïve B cells (P<0.05; 2-sided T-test) analyzed from GSE2350 [29]. *Right panel.* Overlap of selected genes depleted at least 2-fold and overexpressed in MCL versus naïve B cells with pandependent genes [30] and genes associated with MCL poor prognosis [31]. Numbers in green square boxes indicate steps of filtering strategy (see text for details). **b,** Examples of normalized counts of selected sgRNAs on days 0 and 14 from the library screen. **c,** Validation of CEACAM1 gRNAs. Cas9-expressing JEKO-1 cells transduced with control (gNTC) or CEACAM1 gRNAs (gCC1) followed by stimulation with 2 mg/ml of anti-IgM antibody for 5 min and lysates were analyzed by immunoblotting with indicated antibodies. **d,** CEACAM1 is essential in JEKO-1 cells. JEKO-1 cells were transduced with gRNAs as described in (**c**) and fractions of viable, transduced cells co-expressing GFP were monitored over time by flow cytometry. Shown are the means of GFP+ fractions compared to day-2 samples from at least two independent experiments. Error bars, SD. *, $P<0.05$ by a one-sided, paired T test. **e,** Immunoblots of JEKO-1 cells transduced with control or CEACAM1 shRNA and analyzed by indicated antibodies. **f,** Effects of CEACAM1 knockdown on cell survival. Indicated cells were transduced with CEACAM1 shRNA shown in (**e**) and viable, propidium iodide (PI)-negative cells were assessed by flow cytometry over time. Shown are the means of PI negative fractions compared to day-2 samples from at least two independent experiments. Error bars, SD. *, $P<0.05$ by a one-sided, paired T test. **g,** CEACAM1 is required for MCL survival *in vivo*. JEKO-1 cells were transduced with control or CEACAM1 shRNA and equal viable cell numbers (2×10^6) from each group were transferred into each of NSG mice by tail-vein injection. Shown are weekly bioluminescence images of six mice per group. **h,** Line graph showing the measurement of tumor growth *in vivo*. Shown are the means of bioluminescence signals from each group of mice described in (**g**). Error bars, SEM. *, $P<0.05$ by a one-sided T test. **i,** Kaplan-Meier survival analysis of two groups shown in (G) over time. P value by a Log-rank test.

Figure 2

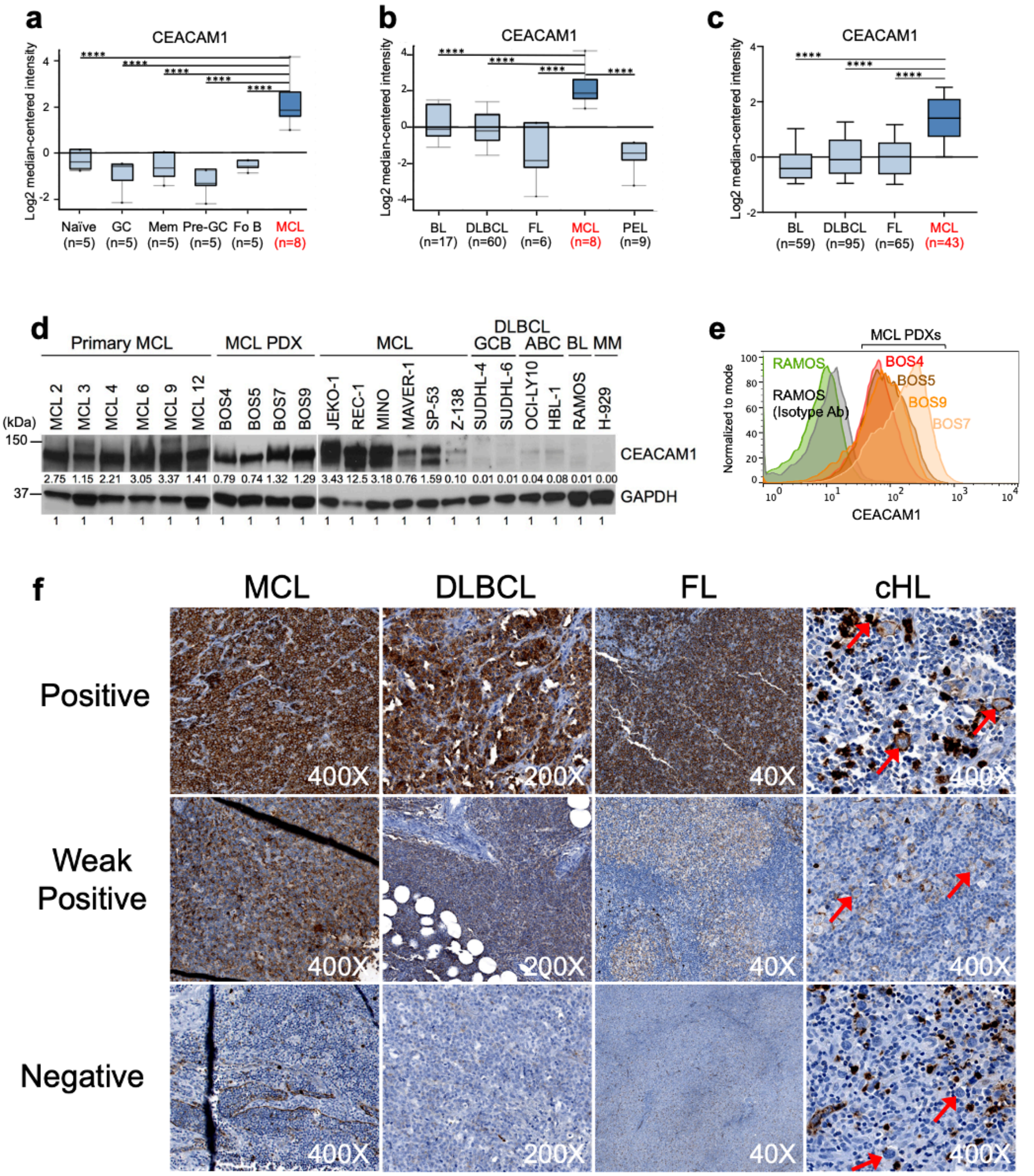

Figure 2

CEACAM1 expression in lymphoma cells. a-c, CEACAM1 mRNA expression levels in MCL and other cell types from the datasets GSE2350 (**a,b**) and GSE132929 (**c**). **** P<0.0001 by a two-sided T test. GC, germinal center; Mem, memory; Fo, follicular; BL, Burkitt lymphoma; DLBCL, diffuse large B-cell lymphoma; FL, follicular lymphoma; PEL, primary effusion lymphoma. **d,** Representative immunoblot analysis of CEACAM1 expression in indicated cells from at least three independent experiments.

Numbers below bands represent densitometric values of CEACAM1 signals normalized over GAPDH loading controls. **e,** Flow cytometry analysis of surface CEACAM1 expression in MCL PDXs compared to CEACAM1-negative RAMOS cells. **f,** Representative immunohistochemistry images showing varying CEACAM1 staining levels for indicated formalin-fixed paraffin-embedded tissue microarrays. See **Table 1** for summary of CEACAM1 positivity in specific diseases. In cHL tissue, background plasma cells are also stained positive.

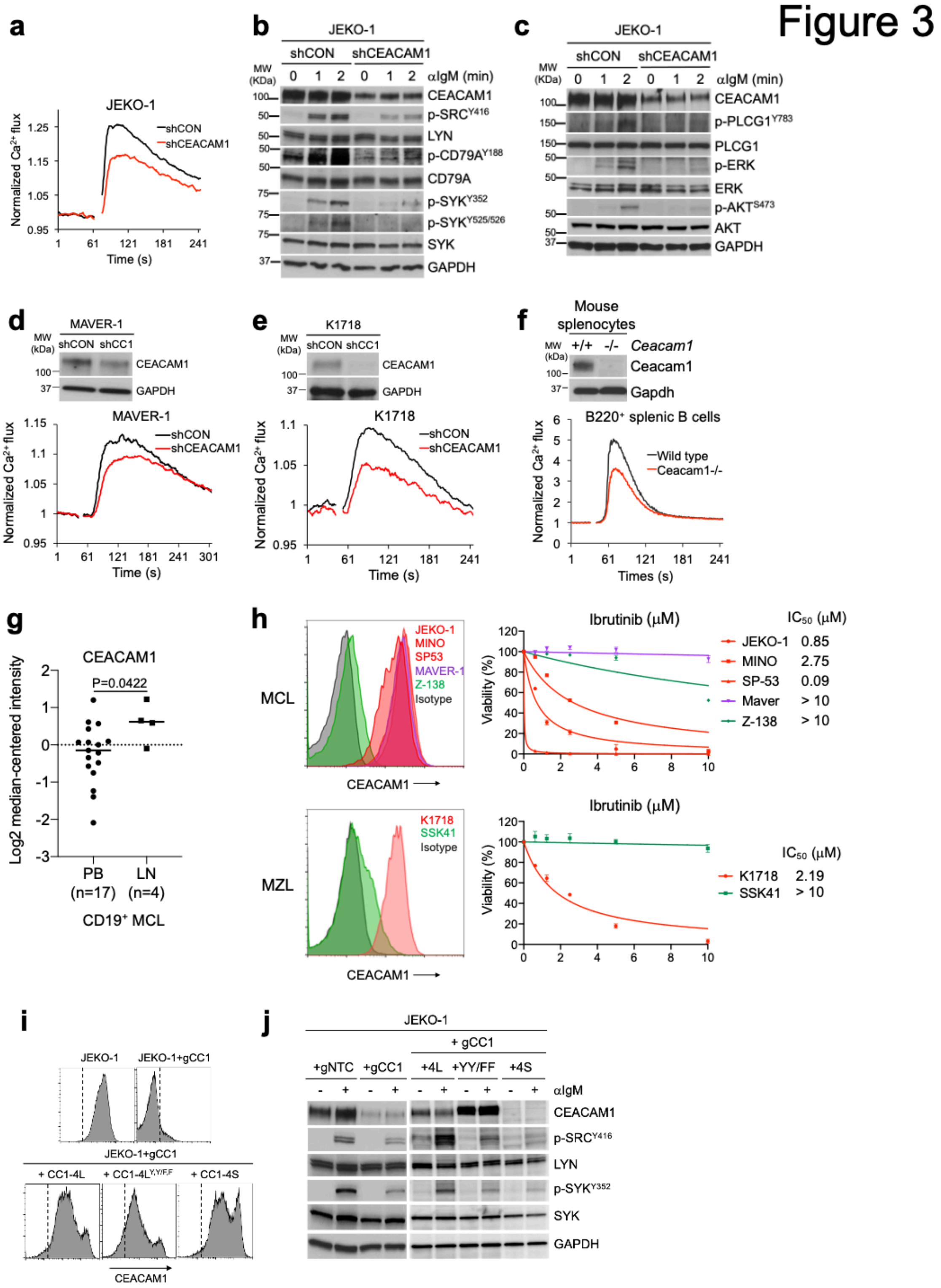

Figure 3

CEACAM1 is required for BCR signaling in MCL. a, Ca^{2+} flux signals in control or CEACAM1 knockdown JEKO-1 cells following anti-IgM stimulation (1 mg/mL) were measured using Indo-1 dye. Shown are arithmetically normalized Ca^{2+} signals using FlowJo Kinetics function. **b,c,** Immunoblot analysis of control or CEACAM1 knockdown in JEKO-1 cells following IgM stimulation (1mg/mL) with indicated antibodies. **d,e,** *Top panels*, immunoblots of indicated cell lines transduced with control or CEACAM1 shRNA with indicated antibodies. *Bottom panels*, Ca^{2+} flux signals in indicated cells transduced with control or CEACAM1 shRNA after IgM stimulation (1 mg/mL). **f,** *Top panel*, immunoblot analysis of splenocytes from wild type (+/+) or Ceacam1 deficient (-/-) mouse with indicated antibodies. *Bottom panel*, Ca^{2+} flux analysis of splenic B cells. Splenocytes from indicated mouse strains were loaded with Indo-1 followed by staining with anti-B220 antibody. Shown are Ca^{2+} signals gated on $B220^{+}$ cells. **g,** CEACAM1 mRNA expression levels in CD19+ sorted MCL cells from peripheral blood (PB) or lymph nodes (LN) analyzed from the GSE70910 dataset [41]. Closed circles or squares represent individual patient samples. Horizontal bars from each group indicate mean mRNA expression. P value is from a two-sided T test. **h,** CEACAM1 expression is correlated with ibrutinib response. *Left panels*, flow cytometry plots showing surface CEACAM1 expression on indicated MCL and MZL cell lines. Isotype, negative control staining for CEACAM1 using Z-138 or SSK41 cells with isotype antibody. *Right panels*, MCL or MZL cell lines response to ibrutinib treatment. Indicated cell lines were treated with indicated doses of ibrutinib for four days and viable propidium iodide (PI)-negative cells were assessed by flow cytometry and normalized to control untreated samples. Line graphs showing means of normalized PI-negative fractions from three independent experiments. Error bars, SD. Fifty percent inhibition concentration (IC_{50}) values were calculated by GraphPad Prism 8 software. **i,j,** ITIM tyrosine residues are required for BCR signaling. JEKO-1 cells transduced with control (gNTC) or CEACAM1 gRNA (gCC1). CEACAM1 knockout cells (gCC1) were reconstituted with WT CEACAM1 (4L), CC1-4L-Y493F/Y520F mutant (YY/FF), or short cytoplasmic tail (4S). Controls or reconstituted cell lines were verified for CEACAM1 expression by flow cytometry (**i**) and stimulated with 1 mg/mL of anti-IgM F(ab')2 fragments for 5 min followed by immunoblot analysis with indicated antibodies (**j**).

Figure 4

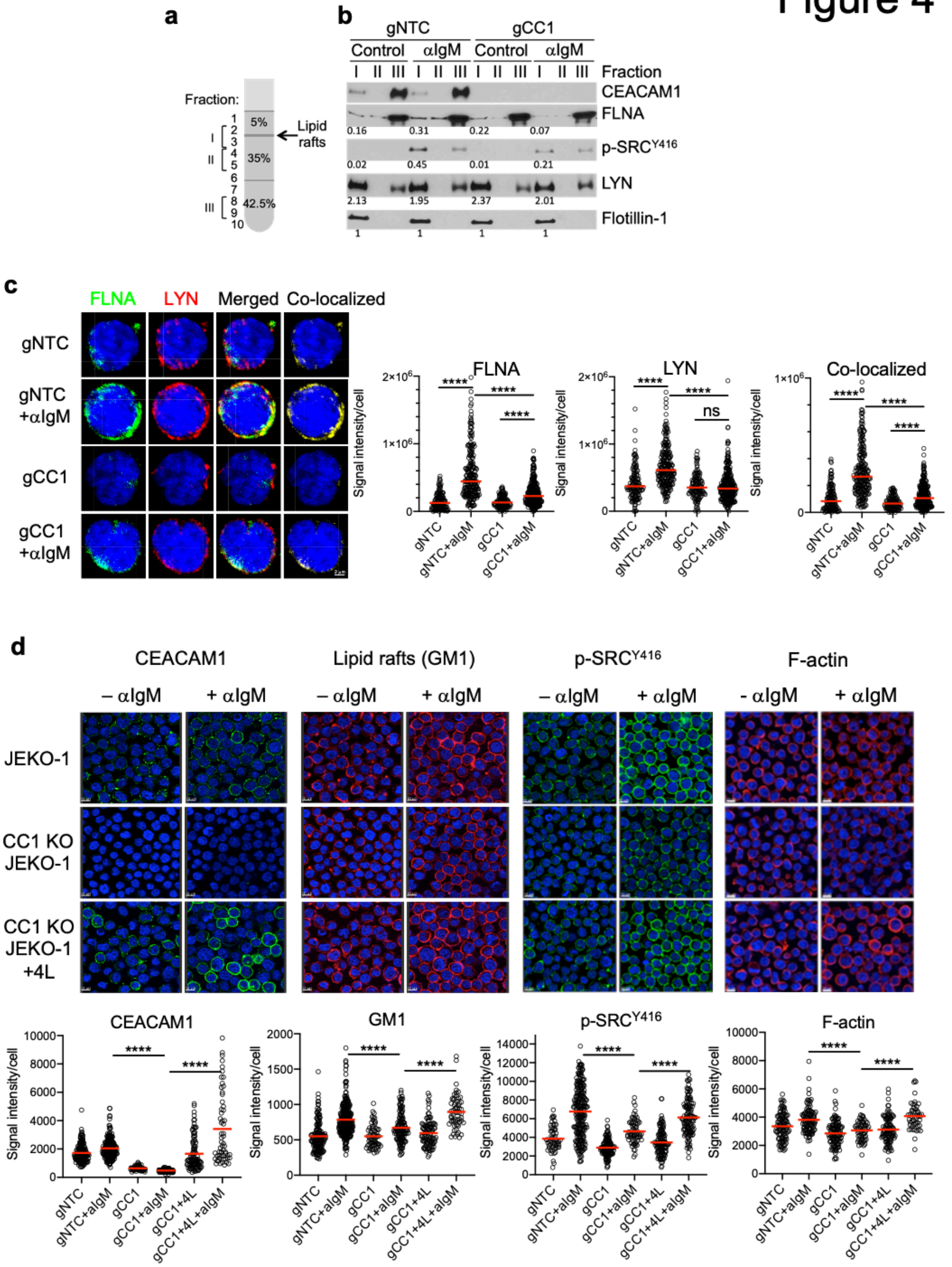

Figure 4

CEACAM1 stabilizes lipid rafts and promotes F-actin reorganization during BCR activation. a, Diagram of sucrose-density gradient fractionation to isolate lipid rafts. **b,** Immunoblot analysis using indicated antibodies for fractions indicated in (**a**) from control or CEACAM1 knockout JEKO-1 cells stimulated with control or anti-IgM antibody (1 mg/ml) for 2 min. Numbers below bands are densitometric values normalized to Flotillin-1 signals. Shown are representative immunoblots from at least two independent fractionation experiments. **c,** *Left panels,* Control (gNTC) or CEACAM1 knockout (gCC1) JEKO-1 cells were stimulated with 2 mg/ml anti-IgM antibody for 2 min. Shown are representative cells from confocal immunofluorescence images (Extended Data Fig. 6) of control and IgM-stimulated cells co-stained with anti-FLNA (green) and anti-LYN (red) antibodies followed by nuclear staining with DAPI (blue). Scale bar, 2 mm. *Right panels,* fluorescent signals from indicated antibodies in each cell from the samples described in (**c**) were quantified using QuPath 0.2.0m6. Shown are the sums of total intensities in all signal-positive areas per cell in arbitrary units. Horizontal red bars indicate the mean. Approximately 200 cells from each sample were analyzed. ****, $P < 0.0001$ by a two-sided T test. ns, not significant. **d,** CEACAM1 is required for optimal assembly of lipid rafts. *Top panels*, Control, CEACAM1 knockout (CC1 KO), or CC1 KO + CEACAM1-4L (4L) JEKO-1 cells were stimulated with 2 mg/ml anti-IgM antibody for 5 min. Shown are representative Airyscan FAST 2D images (acquired with a 40x/1.2NA water objective) of control and IgM-stimulated cells stained with anti-CEACAM1 antibody (green, columns 1 and 2), GM1 via cholera toxin B (red, columns 3 and 4), p-SRC^{Y416} antibody (green, columns 5 and 6), or F-actin via Actin-Stain 555 Phalloidin (red, columns 7 and 8) followed by nuclear staining with DAPI (blue). Scale bar, 10 mm. *Bottom panels*, fluorescent signals from the samples described in the top panels were quantified using QuPath 0.2.0m6. Shown are the sums of total intensities in all signal-positive areas per cell in arbitrary units. Horizontal red bars indicate the mean. Approximately 100 to 200 cells from each sample were analyzed. ****, $P < 0.0001$ by a two-sided T test.

Figure 5

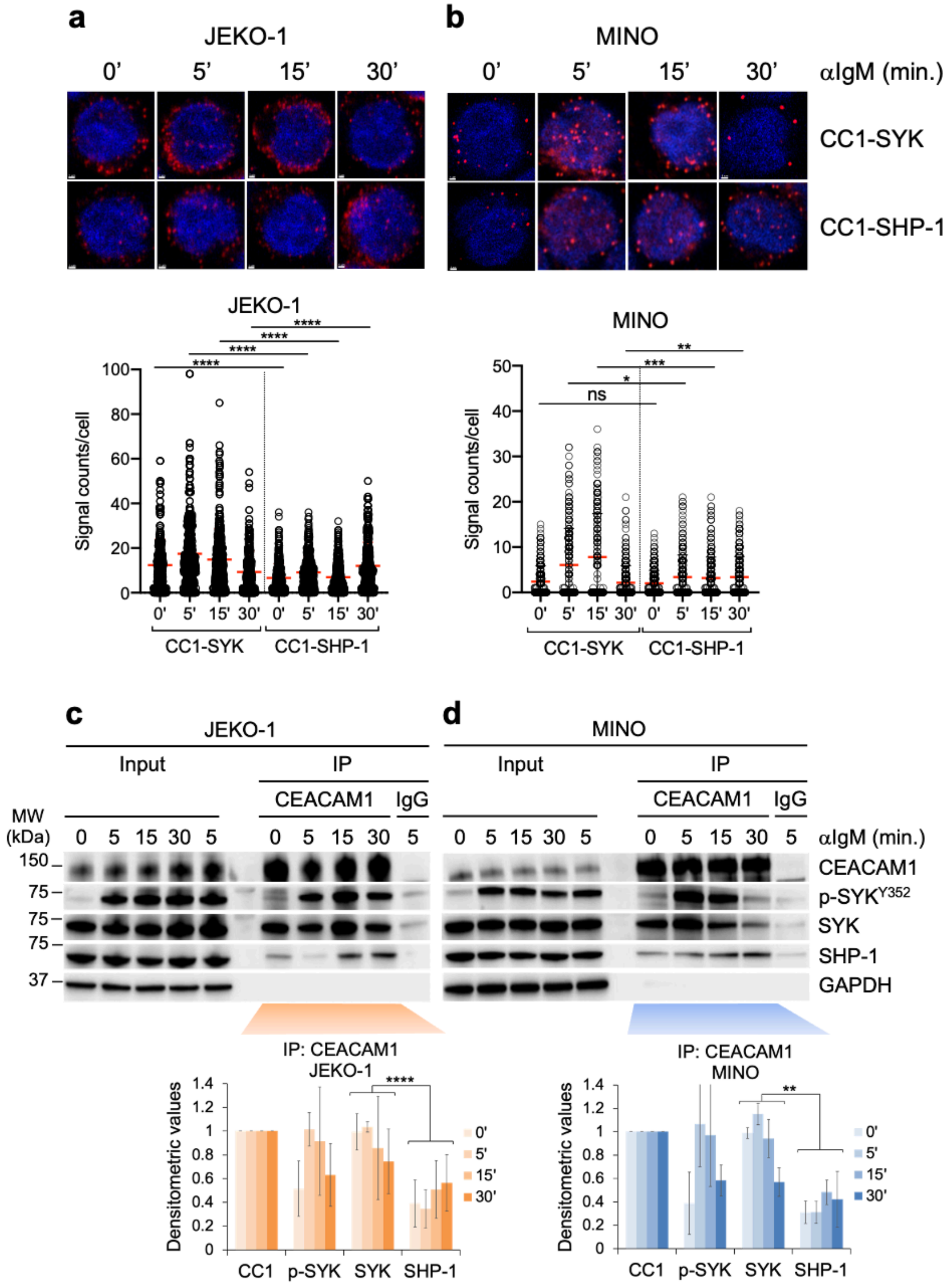

Figure 5

CEACAM1 interactions with BCR signaling components. a,b, *Top panels*, Proximity ligation assay (PLA) showing interactions (visualized as red dots using Airyscan FAST 2D confocal microscope and a 40x/1.2NA water objective) between CEACAM1 (CC1) and the indicated proteins in JEKO-1 and MINO cells stimulated with 2 mg/ml of anti-IgM antibody for the indicated times. *Bottom panels*, Quantitation of PLA signals shown in the top panels for 200−500 cells on average using QuPath 0.3.2 software. ****

P<0.0001, *** P<0.001, ** P<0.01, * P<0.05 by a two-tailed Mann-Whitney U test. ns, not significant. **c,d,** *Top panels*, JEKO-1 or MINO cells were stimulated with 2 mg/ml of anti-IgM antibody for the indicated times and CEACAM1 was immunoprecipitated with a CEACAM1-specific antibody or IgG control antibodies followed by immunoblotting with indicated antibodies. One percent of total lysates was used as input control. *Bottom panels*, Quantitation of the co-IP signals shown in the top panels. Bar graphs show the means of densitometric values from three independent experiments for each timepoint normalized to the CEACAM1 pull-down signals. Error bars, SD. **** P<0.0001, ** P<0.01 by a two-sided nested t test.

Figure 6

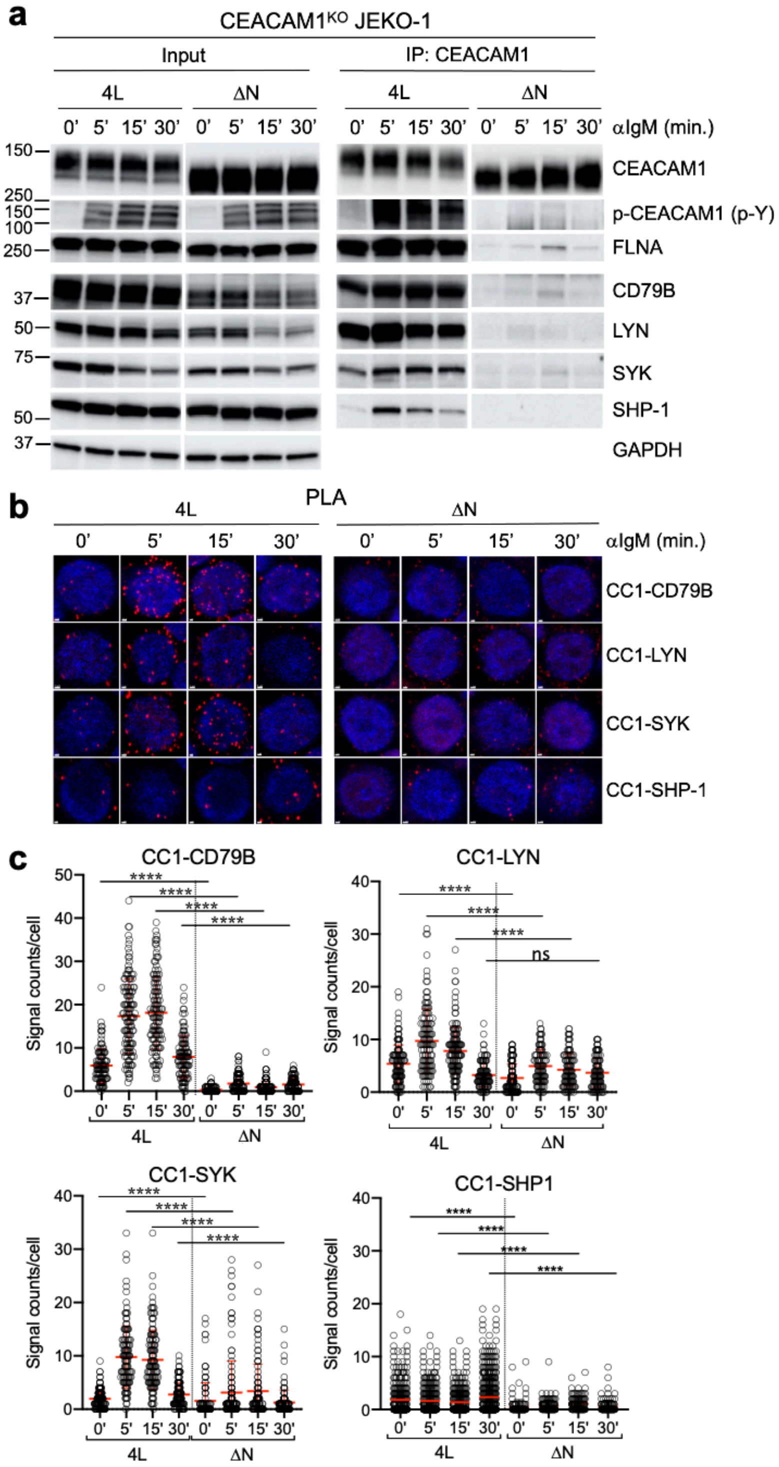

Figure 6

CEACAM1 interactions with BCR signaling components require an intact N-domain. a, CEACAM1-knockout JEKO-1 cells were transduced with either full-length (4L) or N-domain truncated (DN) CEACAM1 constructs, stimulated with 2 mg/ml anti-IgM antibody for the indicated times, followed by CEACAM1 immunoprecipitation and immunoblotting with indicated antibodies. One percent of total lysates was used as input control. **b,** Proximity ligation assay (PLA) showing interactions (visualized as red dots using Airyscan FAST 2D confocal microscope and a 40x/1.2NA water objective) between 4L or DN and the indicated proteins. **c,**Quantitation of PLA signals shown in (**b**) for 100–300 cells on average using QuPath 0.3.2 software. Error bars indicate means with S.D. **** P<0.0001 by two-sided Mann-Whitney U test. ns, not significant.

Figure 7

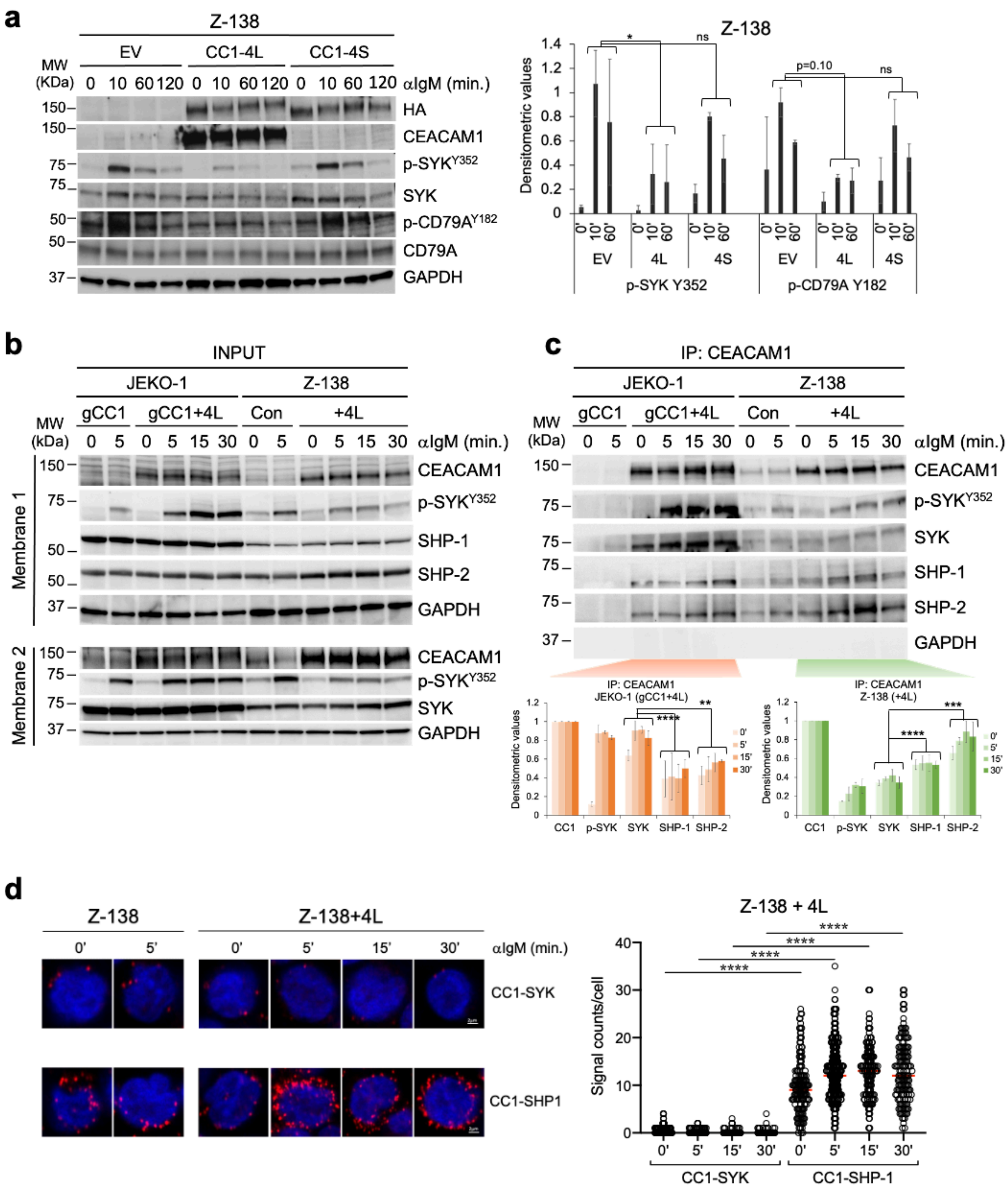

Figure 7

A dual role of CEACAM1 in BCR signaling. a, *Left panel*, CEACAM1 suppresses BCR signaling in Z-138 cells. Z-138 cells were transduced with control empty vector (EV), WT CEACAM1 (CC1-4L), or short cytoplasmic tail CEACAM1 (CC1-4S). Transduced cells were stimulated with 2 mg/mL of anti-IgM F(ab')2 fragments for indicated times followed by immunoblot analysis probed with indicated antibodies. *Right panel*, Quantitation of the immunoblot signals shown in the left panel. Bar graphs show the means of densitometric values from the indicated timepoints normalized to GAPDH loading controls from two independent experiments. Error bars, SD. * $P<0.05$, P values by a two-sided nested t test. ns, not significant. **b,c,** CEACAM1-knockout JEKO-1 cells (gCC1) or Z-138 cells were transduced with either empty vector control or full-length (4L) CEACAM1 construct, stimulated with 2 mg/ml anti-IgM antibody for the indicated times, followed by CEACAM1 immunoprecipitation and immunoblotting with indicated antibodies. One percent of total lysates was used as input control (**b**). Bar graphs show the quantitation of the co-IP signals shown in (**c**). Shown are the means of densitometric values from two independent experiments for each timepoint normalized to the CEACAM1 pull-down signals. Error bars, SD. **** $P<0.0001$, *** $P<0.001$, ** $P<0.01$ by a two-sided nested t test.**d,** *Left panels*, Proximity ligation assay (PLA) showing interactions (visualized as red dots using Airyscan FAST 2D confocal microscope and a 40x/1.2NA water objective) between CEACAM1 (CC1) and the indicated proteins in Z-138 cells or Z-138 cells transduced with CEACAM1-4L followed by stimulation with 2 mg/ml of anti-IgM antibody for the indicated times. *Right panels*, Quantitation of PLA signals shown in the right panels for ~200 cells on average using QuPath 0.3.2 software. **** $P<0.0001$ by a two-sided Mann-Whitney U test.

Figure 8

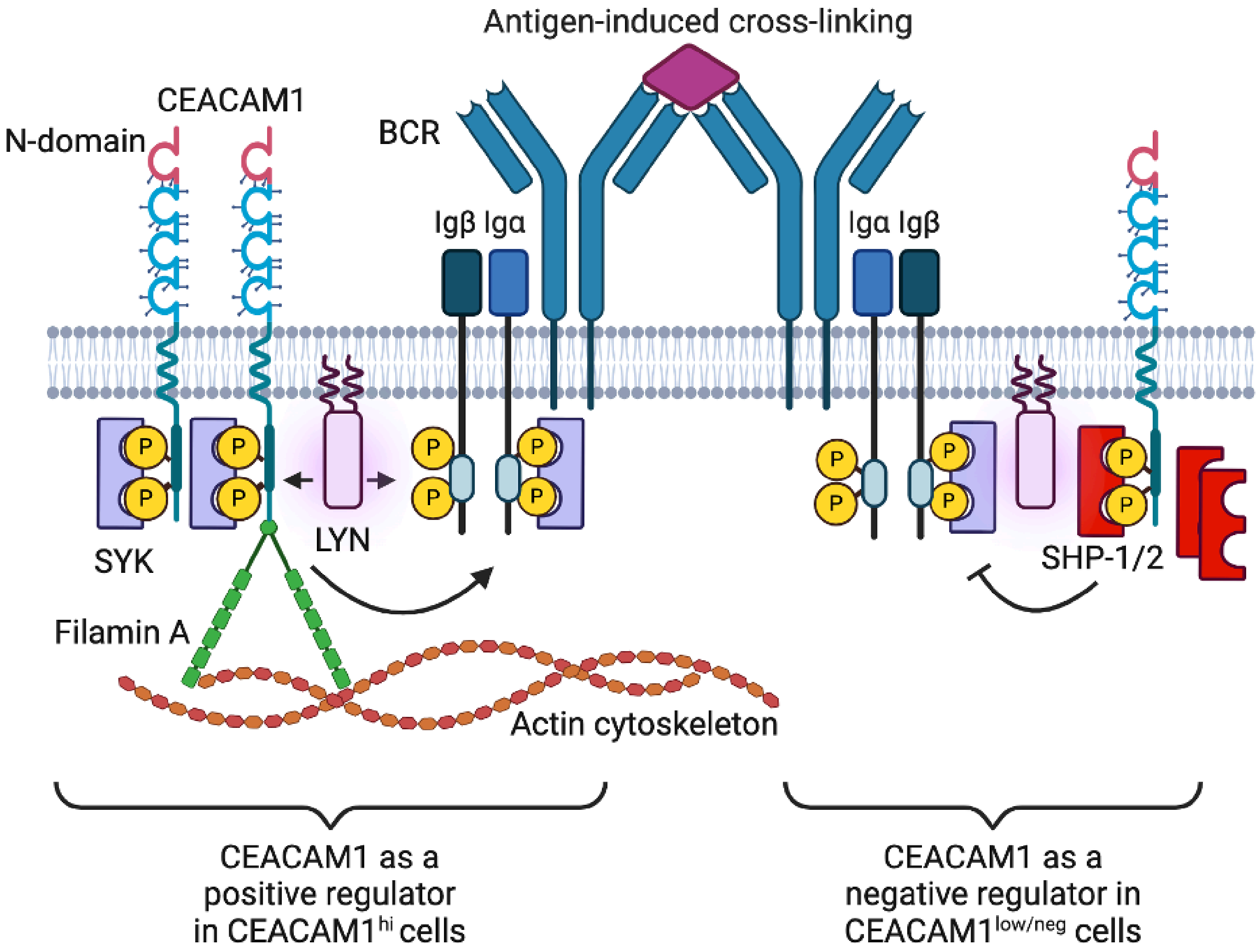

Figure 8

Proposed model for CEACAM1 function in BCR signaling. Following antigen stimulation in B-cell lymphomas with abundant CEACAM1 expression, CEACAM1 binds to FLNA, which anchors to the actin cytoskeleton and stabilizes lipid raft formation, and recruits SYK to the proximity of CD79A/B to enhance BCR activity. In cells with low or no CEACAM1 expression (and potentially low SYK expression), SHP-1 and SHP-2 outcompete for CEACAM1 binding, leading to signal attenuation. Created with BioRender.com.

Supplementary Files

This is a list of supplementary files associated with this preprint. Click to download.

- SupplementaryMaterialsS220241023.pdf

- SupplementaryMaterialsS220241023.pdf
- SupplementaryTable120241023.xlsx
- SupplementaryTable220241023.xlsx
- SupplementaryTable320241023.xlsx
- SupplementaryTable456720241023.xlsx
- SupplementaryTable820241023.xlsx
- SourcedataExtendeddataFig.1B.pdf
- SourcedataExtendeddataFig.1C.pdf
- SourcedataFig1CDFHIImmunoblotsstatistics.xlsx
- SourcedataFig2Cstatistics.xlsx
- SourcedataFig3BCGHJImmunoblotsStatisticsIC50.xlsx
- SourcedataFig4CDStatistics.xlsx
- SourcedataExtendeddataFig.5ACimmunoblotsstatistics.xlsx
- SourcedataFig5ABCDIFdensitometryimmunoblotsstatistics.xlsx
- SourcedataFig6ABCImmunoblotsconfocalIFstatistics.xlsx
- SourcedataExtendeddataFig.7.pdf
- SourcedataFig7ACDdensitometryimmunoblotsIFstatistics.xlsx
- SourcedataExtendeddataFig8statistics.xlsx
- SourcedataExtendeddataFig10Immunoblotsstatistics.xlsx